DOI: 10.1002/smll.200500256

Near-Edge X-ray Absorption Fine Structure Spectroscopy as a Tool for Investigating Nanomaterials

*Tirandai Hemraj-Benny, Sarbajit Banerjee, Sharadha Sambasivan, Mahalingam Balasubramanian, Daniel A. Fischer, Gyula Eres, Alexander A. Puretzky, David B. Geohegan, Douglas H. Lowndes, Weiqiang Han, James A. Misewich, and Stanislaus S. Wong**

***We** have demonstrated near-edge X-ray absorption fine structure (NEXAFS) spectroscopy as a particularly useful and effective technique for simultaneously probing the surface chemistry, surface molecular orientation, degree of order, and electronic structure of carbon nanotubes and related nanomaterials. Specifically, we employ NEXAFS in the study of single-walled carbon nanotube and multi-walled carbon nanotube powders, films, and arrays, as well as of boron nitride nanotubes. We have focused on the advantages of NEXAFS as an exciting, complementary tool to conventional microscopy and spectroscopy for providing chemical and structural information about nanoscale samples.*

Keywords:
- carbon nanotubes
- functionalization
- nanomaterials
- NEXAFS spectroscopy
- surface analysis

1. Introduction

It is recognized that nanoscience will play an increasingly significant role in technological developments in this century. Nanomaterials, the dimensions of which are on the nanometer scale, such as single-walled carbon nanotubes (SWNTs) and quantum dots, exhibit unique size-dependent physical and chemical properties. These demonstrate many potential applications in fields as diverse as molecular electronics, actuators, gas storage, tips for scanning probe microscopy, nanocatalysis, field emission, and high-strength composite materials.[1–4] Although SWNTs have mostly been the focal point of attention, other nanostructures, such as boron nitride nanotubes, which also exhibit a similar graphitic-like layered structure, have also shown similar potential applications.[5,6]

Many of these proposed applications require that these functional nanoscale materials be controllably incorporated into complex architectures such as three-dimensional arrays, where, for instance, the anisotropic properties (such as quantum confinement) of SWNTs can be more readily exploited as compared with those of bulk samples. Moreover, in order for these nanomaterials to attain their full potential, control of nanoscale alignment, purity, and functionalization needs to be demonstrated. Progress in the rational chemical functionalization of SWNTs with oxygenated functional groups has enabled their solubilization, individualization, purification, separation on the basis of diameter and electronic structure, and subsequent assembly.[7–11] Indeed,

[*] T. Hemraj-Benny, Dr. S. Banerjee, Prof. S. S. Wong
Department of Chemistry
State University of New York at Stony Brook
Stony Brook, NY 11794-3400 (USA)
Dr. S. Sambasivan, Dr. D. A. Fischer
Materials Science and Engineering Laboratory, National Institute of Standards and Technology, Gaithersburg, MD 20899 (USA)
Dr. M. Balasubramanian
Sector 20, Advanced Photon Source
Argonne National Laboratory; Argonne, IL 60439 (USA)
Dr. G. Eres, Dr. A. A. Puretzky, Dr. D. B. Geohegan, Dr. D. H. Lowndes
Condensed Matter Sciences Division
Oak Ridge National Laboratory
Oak Ridge, Tennessee 37831 (USA)
Dr. W. Han
Center for Functional Nanomaterials
Brookhaven National Laboratory; Upton, NY 11973 (USA)
Dr. J. A. Misewich, Prof. S. S. Wong
Materials Sciences Department, Brookhaven National Laboratory
Bldg. 480, Upton, NY 11973 (USA)
Fax: (+1) 631-632-7960
E-mail: sswong@notes.cc.sunysb.edu

the roadmap to generating practical functional materials involving nanotubes, as well as for other nanoscale building blocks, necessitates a) controllable synthesis in terms of monodispersity, surface chemistry, and dimensionality, b) rigorous characterization and understanding of structure–property relationships, and c) alignment and controllable positioning of these materials in devices and architectures.

Nevertheless, there is still much to be done, since the majority of SWNTs tend to be formed as heterogeneous materials, that is, with varying diameters, lengths, bundling characteristics, and chiralities. Hence, it is critical that we improve upon and otherwise develop new means of characterizing SWNTs and other nanostructures. In effect, there is a need for a nondestructive tool to probe not only the nature of surface functional groups on these tubes, but also the structural and electronic properties of these tubes.

Most traditional spectroscopic techniques are incapable of simultaneously probing chemical bonding, surface molecular orientation, and electronic structure. For instance, infrared spectroscopy has been used to study the chemical nature of oxygenated, functionalized carbon nanotubes, where it mainly analyzes the nature of surface moieties. The highly symmetric structure of the nanotubes implies that few modes of the nanotube itself are IR-active. Thus, incredibly surface-sensitive techniques such as photoelastic modulated infrared spectroscopy and attenuated total reflectance spectroscopy are limited to studying functional groups on nanotube surfaces.

Raman spectroscopy has been a sensitive probe of electronic structure in nanotubes and is often used to study disorder or sidewall functionalization. However, the Raman spectra of carbon nanotubes are strongly resonance-enhanced, and thus, signals emanating from functionalizing moieties themselves rarely appear in Raman spectra.[7,12] Raman spectroscopy has been found to be a useful probe of alignment and structure in nanotubes. However, there have been several complications related to the interpretation of Raman data of carbon nanotubes. More specifically, the intensity of the disordered D band is dispersive and depends on the laser-excitation wavelength used to probe the sample. Also, varying intensity changes in the D band have been reported for similar degrees of sidewall functionalization, which is associated with the dramatic difference expected for Raman cross sections for sp^2- versus sp^3-hybridized carbon atoms. Other complications, related to the interpretation of Raman data of functionalized SWNTs, relate to the data's dependence on sample purity as well as to its insensitivity to small amounts of oxidation, particularly at the ends and defect sites.[13,14]

Whereas X-ray photoelectron spectroscopy (XPS) can differentiate amongst and quantify various types of functional groups on a nanotube surface, details of nanotube alignment are often difficult to extract from these data. Conversely, while diffraction techniques may provide insight into nanotube alignment, analysis of diffraction data is often rendered difficult by scattering from catalyst impurities ubiquitous in the vast majority of nanotube samples. Microscopy techniques, such as transmission electron microscopy and scanning tunneling microscopy, are effective local probes of nanotube structure and morphology but are not sufficient in terms of developing a detailed quantitative understanding of properties of bulk samples.

Therefore, it is obvious that complementary additional techniques are important in obtaining a more comprehensive understanding of SWNTs. In recent years, our group has strenuously pursued near-edge X-ray absorption fine structure spectroscopy (NEXAFS) as a means of investigating chemical bonding, electronic structure, surface chemistry, and the degree of alignment of SWNTs. We have focused on the advantages of NEXAFS as a complementary tool to microscopy and other spectroscopies for providing chemical, structural and orientational information about nanoscale samples.

1.1. Principles of NEXAFS

NEXAFS involves the excitation of electrons from a core level to partially filled and empty states. The decay of core hole states results in the emission of Auger electrons from valence molecular orbitals, resulting in a NEXAFS electron yield spectrum (Figure 1A). Hence, the peak positions and spectral lineshape in a NEXAFS spectrum are directly related to the nature of these unoccupied electronic states. Decay of core holes may also occur via the emission of fluorescent photons, which originate from the top 200 nm of the film as opposed to Auger electrons, which arise from the top 10 nm. Thus, this technique is both surface and bulk sensitive and is capable of probing both nanotube electronic structure as well as surface functional groups simultaneously.

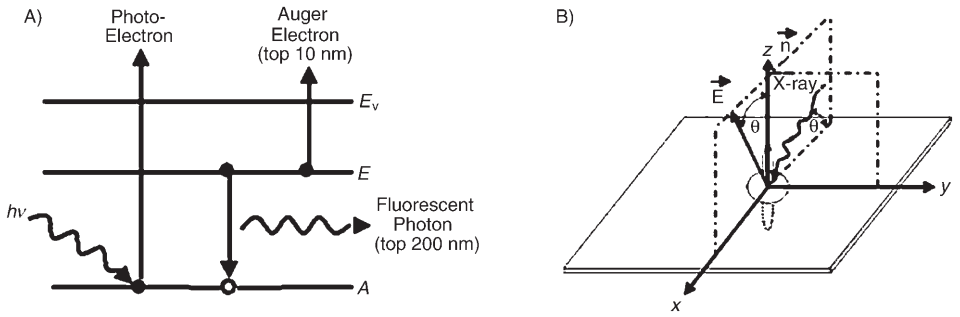

Figure 1. A) Schematic representation of the basic theory of NEXAFS. The target atom absorbs an X-ray photon and emits a core electron from, for example, the K (1s) or L (2p) shell, which propagates outwards to an unoccupied discrete level, thereby creating a core hole. An electron from a higher energy level fills the hole, releasing excess energy either by the radiation of fluorescence photons (bulk sensitive) or by the emission of Auger electrons (surface sensitive). NEXAFS spectra are recorded by measuring either the electron yield or fluorescence yield as a function of incident photon energy. B) Representation of the geometry of π* vector orbitals (vertical to the *xy* plane) and σ* planes (within the *xy* plane) with respect to the incident beam and the electric field vector, **E**, which remains perpendicular to the incident X-ray irradiation.

In the context of carbon-based structures such as SWNTs, NEXAFS measurements can detect specific bonds in molecules (e.g., C=C, C–C, and C–O bonds)[15] as well as the angular dependence of the specific orbitals involved. The detailed spectral resonances at the carbon K-edge, for instance, yield information about the bonding environment of carbon atoms in the sample, such as the presence of functionalized species and chemisorbed impurities.

In addition, while the position of the σ resonance is a measure of the intramolecular bond length, the location and intensity of the lower-energy π* resonance can provide insights into bond hybridization. The transitions, namely, 1s→π* and 1s→σ*, can be thought of as dipole transitions from initial s states to the p component of the π* and σ* final states, respectively. It is thus possible to distinguish between sp^2 and sp^3 bonding from the symmetry of the final state, since the former is π-like while the latter is σ-like.

The transition matrix elements also have an angular dependence on the angle made by, for instance, the π* orbital with respect to the electric field vector of the incident-polarized X-rays. Since the light from the synchrotron source used is linearly polarized, the intensity of the π* and σ* transitions will be sensitive to the orientation of these orbitals with respect to the polarization vector. Therefore, changes in the intensity of resonances upon rotating the sample in the plane of incidence of the beam provide evidence for bond orientation (Figure 1B).[15,16]

1.2. Electronic and Structural Analysis of Nanotubes by NEXAFS

We and others[13,17–20] have shown that NEXAFS spectroscopy can be used to determine: 1) the presence of defects and amorphous content in carbon nanotubes; 2) varying degrees of bond hybridization in mixed sp^2/sp^3-bonded carbon materials; 3) the degree of vertical alignment in nanotube samples; and 4) the nature of oxygen-containing functional groups on nanotube surfaces. Specifically, our group has utilized NEXAFS to probe: 1) the effect of ozonation on the surface chemistry and electronic structure of both SWNTs and multi-walled carbon nanotubes (MWNTs);[21,22] 2) the nature of crystallographic phases of boron nitride nanotubes as well as the presence of defects and degree of crystallinity in these nanoscale samples;[23] and 3) both quantitative and qualitative evaluations of order and alignment in carbon-nanotube-based systems.[24] Herein, we will focus on the details of our work and on the importance of NEXAFS spectroscopy as a unique complementary technique in investigating the electronic, orientational, and structural properties of nanotube-based systems.

1.3. Data Collection and Processing

All C K-edge, O K-edge, B K-edge, and N K-edge NEXAFS spectra reported here were taken at the U7A NIST/DOW end station at the National Synchrotron Light Source (NSLS) at Brookhaven National Laboratory.[21–24] The partial electron yield (PEY) signal was collected using a channeltron electron multiplier with an adjustable entrance grid bias (EGB). A variable negative bias in the range of 20–200 V was applied to reject extraneous background due to low-energy electrons. The use of different biases allowed for both top-surface and bulk (up to 10 nm) analyses. Data were recorded in a UHV chamber, at room temperature, with an incident X-ray resolution of 0.1 eV. Spectra were collected at different polarization angles by rotating the sample holder with respect to the incident beam in the plane of incidence. The monochromator energy was calibrated using the carbon K-edge π* transition of graphite, located at 285.35 eV. To eliminate the effect of fluctuations in the incident beam intensity and of monochromator absorption features, the PEY signals were normalized using the incident beam intensity obtained from the photoemission yield of a clean Au grid with 90% transmittance.

All spectra were processed through standard pre- and post-edge normalization methods. Details can be found in previously published work.[21–24] Thus, changes in the spectral intensity observed arise from chemical changes or anisotropy in the system and are independent of the total carbon content. For the polarization studies of carbon nanotube arrays, a comparison of intensities at different polarization angles and for different samples was made by subtracting an arctangent function to account for the C K-edge jump, after which the π* and σ* resonances were fitted to Gaussian functions. Peak areas from the π* and σ* resonances as a function of incident beam angle were used to calculate the degree of orientation of the carbon nanotubes.

2. Probing Sidewall-Functionalized MWNTs and SWNTs

We have demonstrated that NEXAFS is a useful and powerful probe of the covalent functionalization of carbon nanotubes, wherein the nature of the tube electronic structure and the chemical functional groups introduced can be monitored simultaneously. Our results suggest that NEXAFS can effectively serve as a complementary tool to vibrational spectroscopy in characterizing pristine and functionalized carbon nanotubes, including both SWNTs and MWNTs.

2.1. SWNTs

Specifically, we have carried out a comparative NEXAFS study[21] of both pristine and various surface-oxidized single-walled carbon nanotubes, including a) wet-air oxidized tubes, in addition to b) ozonized tubes whose sidewalls have been covalently functionalized with oxygenated functionalities.[25] Solution-phase ozonized tubes have been used as templates for the synthesis of nanotube–quantum dot heterostructures as well as for the self-assembly of nanotubes onto metal surfaces.

By monitoring π* and σ* transitions, as observed from the C K-edge and O K-edge (Figure 2A and B, respective-

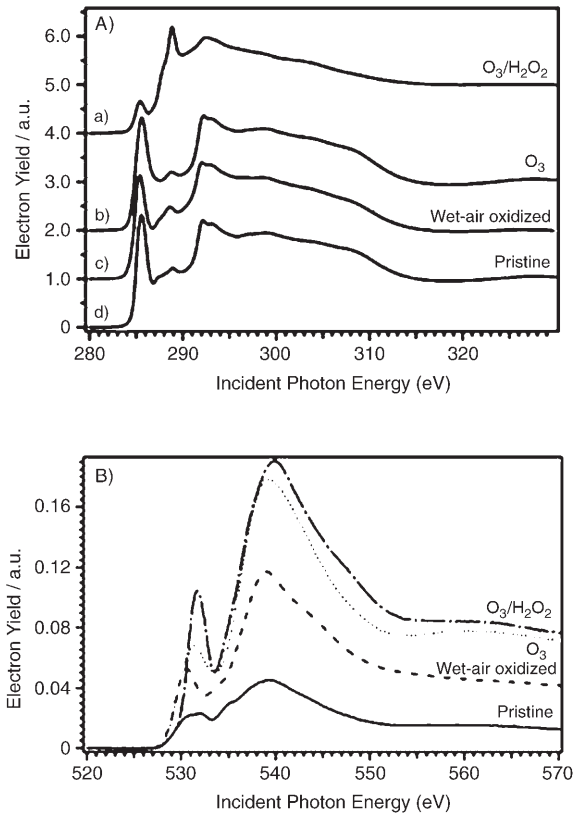

Figure 2. A) C K-edge spectra of SWNTs, prepared by a) O_3/H_2O_2 treatment; b) O_3-treated HiPco SWNTs; c) wet-air-oxidized HiPco SWNTs; and d) pristine HiPco SWNTs. B) O K-edge spectra of SWNTs, prepared by O_3/H_2O_2 treatment, O_3-treated HiPco SWNTs, wet-air-oxidized HiPco SWNTs, and pristine HiPco SWNTs, respectively from top to bottom. O K-edge spectra are pre-edge subtracted; no step normalization has been performed. Adapted from Ref. [21].

ly), one can determine the extent of oxidation, and thus the level of sidewall functionalization. For instance, it was observed that as the tubes were increasingly oxidized (from raw to ozone/H_2O_2-treated samples), there was a diminution of the first nanotube π*-peak intensity (at 285.4 eV) with respect to the strength of the σ*-peak intensity (Figure 2A). This result is consistent with the loss of the characteristic electronic transitions between the intrinsic van Hove singularities of functionalized, ozonized nanotubes, which is due to the disruption of the inherent π-network upon sidewall functionalization, as has been observed with previous data obtained from Raman and near-IR/UV-Vis spectroscopies.[25] Recent transport results further provide evidence for the introduction of scattering centers on nanotube sidewalls upon ozonation, consistent with this view of functionalization.[26]

More specifically, the fitted C K-edge spectrum of sidewall-oxygenated nanotubes was characterized by a sharp C–C π* transition at 285.4 eV, three C–H and C–C σ* transitions from 289.9–298 eV, and broad σ+π transitions from 301–309 eV. The two additional peaks within the 287–290 eV region can be respectively assigned to π* C=O and σ* C–O transitions of the oxygenated functionalities.[21]

In addition, one can also obtain valuable information about the degree of functionalization (oxidation) of carbon nanotubes from the edge jump of the O K-edge spectra, which is proportional to the total oxygen content. For instance, as observed in Figure 2B, there is an increase in the edge-jump intensity with the expected order of increasing oxidation from pristine tubes, next to wet-air-oxidized tubes, and finally, onto oxidized sidewall carbon atoms of ozone/H_2O_2-treated tubes. The pre-edge normalized O K-edge spectra for the pristine and functionalized carbon nanotubes showed characteristic peaks at 532 eV (which can be assigned to a π* C=O transition) and at 538–542 eV (which are broader, asymmetric peaks and are associated with σ* C–O transitions). One should also note that the O K-edge profile and intensity of the peaks differ amongst the various types of pristine, air-oxidized, ozonized, and ozone/H_2O_2-treated nanotubes. This corresponds to the presence of various types of oxygenated functionalities, such as carboxylic acids and keto groups, as confirmed by infrared spectroscopy and XPS results.[21]

2.2. MWNTs

We have also monitored the nature of oxygen-bearing functionalities on functionalized, ozonized MWNTs by means of NEXAFS. Specifically we have demonstrated and confirmed previous data that the outer walls of MWNTs are oxidized to a greater extent than the inner walls. This information was obtained by varying the retarding potential, thereby enabling surface depth profiling. Figure 3A shows the NEXAFS spectra for pristine and ozonized nanotubes, obtained with a retarding potential of −200 V for high surface sensitivity. Figure 3B shows data for similar samples at −20 V, which probes the surface and a few interior layers. Since the low-energy inelastic electrons from the bulk cannot reach the detector at the higher retarding potential, we noted that the C=O π* and C–O σ* transitions in the 287–290 eV region in Figure 3B originated after ozonation and that these transitions were weaker than those observed at a retarding potential of −200 V. This is consistent with TEM and XPS data, which show that the outer layers of the MWNTs are mainly reacting with ozone and which can be explained based on the fact that there is a lack of accessibility of ozone to the inner walls.[22]

It should be further noted that from the C K-edge of the MWNTs (Figure 3), the π* intensities are attenuated but not as extensively, as was previously seen with data associated with the sidewall functionalization of SWNTs. In addition, the presence of oxygenated functionalities observed in our NEXAFS data (i.e., ketones, carboxylic acids, and alcohols) was confirmed by attenuated total reflection (ATR)-IR and O K-edge data (Figure 3C and D, respectively).[22] MWNTs are intrinsically larger than SWNTs. Because only the outermost shells of MWNTs are exposed to ozone, our results suggest that ozonolysis of larger-diameter MWNTs leads to significantly lower oxidation as compared with the more highly reactive (and incidentally, more highly curved), smaller-diameter SWNTs. Therefore, in MWNTs, it is ex-

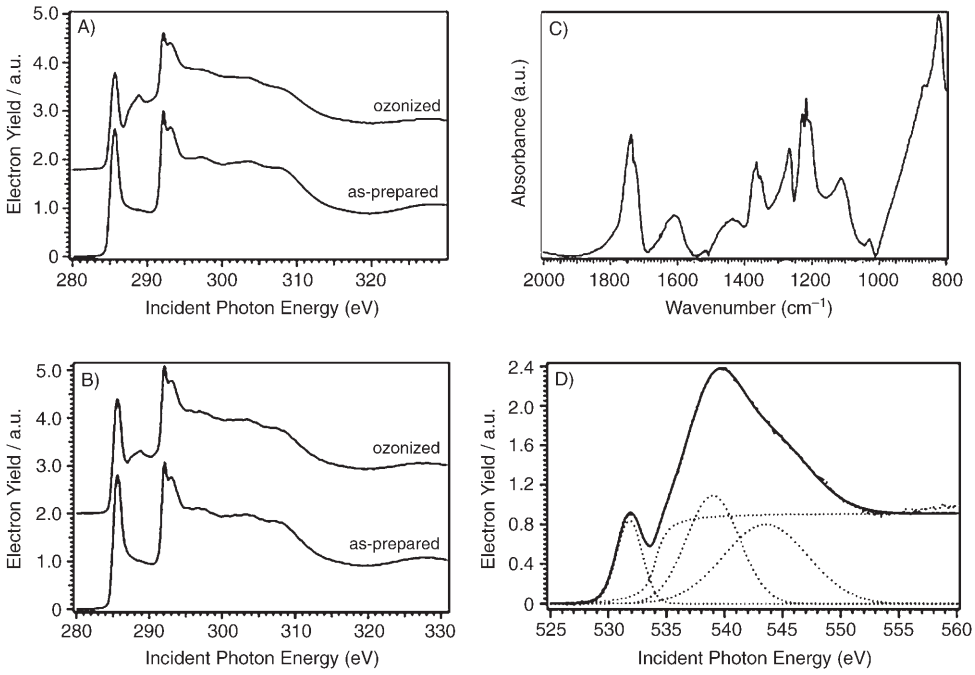

Figure 3. A, B) C K-edge spectra, taken at retarding potentials of −200 V (A) and −20 V (B). The lower spectra in A) and B) represent the as-prepared MWNTs. The top spectra correspond to those of the ozonized MWNTs. All the spectra have been pre- and post-edge normalized, as described in the text. C) Attenuated total reflection (ATR) FT-IR spectrum of ozonized MWNTs. D) Fitted O K-edge spectra for ozone-treated multiwalled nanotubes indicating the positions of major component peaks. Measured spectra (dash-dotted line), fitted spectra (solid line), and fitted component peaks (dotted line) are shown. See text for assignments. Adapted from Ref. [22].

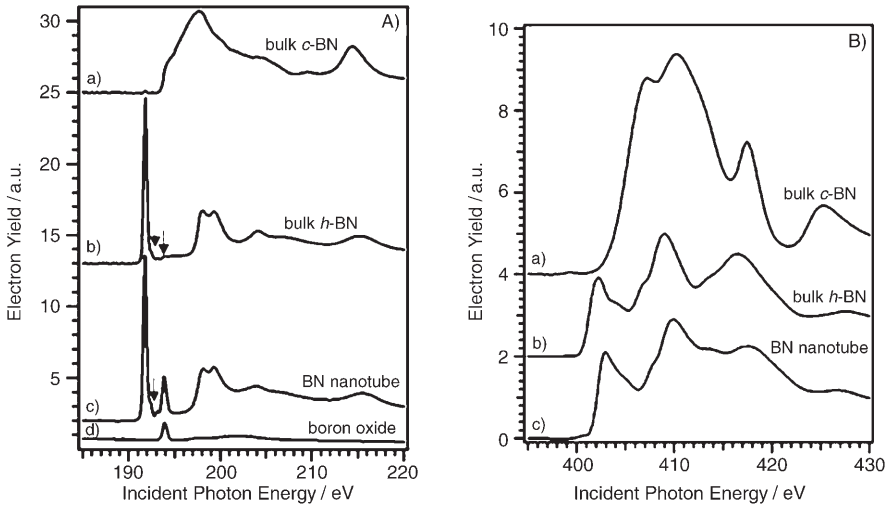

Figure 4. A) B K-edge spectra, taken at a retarding potential of −50 V and at the magic angle (θ = 54.7°): a) bulk c-BN sample; b) bulk h-BN sample; c) BN nanotube samples; d) boron oxide sample. B) N K-edge spectra, taken at a retarding potential of −50 V and at the magic angle (θ = 54.7°): a) bulk c-BN sample; b) bulk h-BN sample; c) BN nanotube samples. All spectra have been pre- and post-edge normalized as described in the text. Adapted from Ref. [23].

pected that ozone reactions are spatially localized at the end caps and defect sites, due to the end caps having higher curvature, which render them more reactive than the sidewalls.[10,22,27] Thus, NEXAFS is seen to verify predictions of the curvature-dependent reactivity of nanotubes, arising from pyramidalization and π-orbital misalignment considerations.[10,28]

3. Probing Boron Nitride (BN) Nanotubes

Some techniques commonly used in distinguishing zinc-blende cubic (c-BN) from hexagonal (h-BN) phases of boron nitride in bulk, and thus, sp^3 from sp^2 hybridization, include X-ray diffraction (XRD), Raman spectroscopy, infrared spectroscopy (IR), electron energy loss spectroscopy (EELS) and NEXAFS. However, it is generally found that vibrational spectroscopies and XRD are not suitable for studying the structure of nanocrystalline samples due to phonon confinement and Scherrer broadening effects, respectively. On the other hand, NEXAFS has the intrinsic advantage of being a nondestructive analytical tool and is inherently more sensitive to the bonding configurations of the different types of atoms, making it a more localized technique. We have used NEXAFS to differentiate between nanoscale hexagonal BN and cubic BN and furthermore, we have probed the presence of defects and the degree of crystallinity in these nanoscale samples.

We have demonstrated NEXAFS as an effective tool in investigating the structure of a boron nitride nanotube.[23] Specifically, it was confirmed by NEXAFS that a sample of boron nitride nanotubes[23,29,30] indeed consisted predominantly of hexagonal BN nanotubes (sp^2 hybridization), and thus, it is expected to exist in graphitic-like layer forms. The B K-edge and N K-edge (Figure 4 A and B, respectively) of the BN nanotubes (curve c) showed similar features to those of bulk h-BN (curve b).

The prominent, narrow, and intense peak at 191.8 eV corresponds to a B 1s→ π* resonance, consistent with sp^2-hybridization and planar bonding. Two nearby resonances at around 198.5 and 199.7 eV were correlated with the excitation to a single, energy-split σ* state. The peak at 193.8 eV originated from

unreacted boron oxide, which is a precursor for BN nanotubes. In addition, it was confirmed that these BN tubes are highly crystalline and have a low defect density. Two peaks, noted at 192.4 and 193 eV from the B K-edge, were attributed to defects in the hexagonal bonding, more specifically with boron atoms bonded to either one or two nitrogen atoms, though these were relatively small and shoulder-like in their appearance.[23] Thus, it was assumed that the studied sample of BN nanotubes synthesized by a high-temperature carbon nanotube substitution method is highly crystalline with the presence of a minimum level of defects, as could also be confirmed by TEM and XRD data.[29] The B K-edge data of bulk cubic c-BN sample, shown in curve a, possessed no detectable π* features at 191.8 eV present in the B K-edge, which would have arisen from a predominant sp^2 hybridization.

4. Probing Alignment in Carbon Nanotube Systems

As mentioned previously, it is likely that many functional nanoscale materials will require the controllable incorporation of multiple carbon nanotubes into arrays. For example, the mechanical properties of composite materials for high-strength applications are optimized by increasing the ordering of nanotubes in fibers or films.[31,32] Moreover, the fabrication of vertical arrays with controlled nanotube densities is critical for field-emission applications. Although there have been many methods of fabricating ordered nanotube systems,[32–35] the problem of characterizing order and alignment in these arrays has not been trivial.

Whereas techniques such as polarization Raman spectroscopy, polarized absorption spectroscopy and X-ray scattering can be used to characterize alignment,[36–38] these methods possess limitations. For example, since Raman spectroscopy is very sensitive to the electronic structure of carbon nanotubes, Raman intensities can be greatly affected by factors such as surface modification, charge transfer, strain, and degree of aggregation in bundles.[7,39]

NEXAFS spectroscopy has been previously used to investigate order and alignment in many arrays, including carbon nanotube arrays.[18] In addition, we have demonstrated that this technique can be used to qualitatively and quantitatively investigate the degree of order and alignment in a wide range of carbon nanotube-based systems.[24,40] These have included SWNT powders, SWNT films, as well as aligned SWNTs and MWNTs.[24,40]

4.1. HOPG

In order to fully understand polarization trends for carbon nanotube samples, we initially consider NEXAFS of a particularly ideal system, that is, highly ordered pyrolytic graphite (HOPG). Typical C K-edge spectra, where the changes in NEXAFS partial electron yield (PEY) intensities at different incident angles are plotted, can be seen in Figure 5A. The first π* resonance occurs at 285 eV and broad σ* resonances occur in the region from 290 to 315 eV.[15,24] As seen in the inset of Figure 5A, all of the π* orbitals are

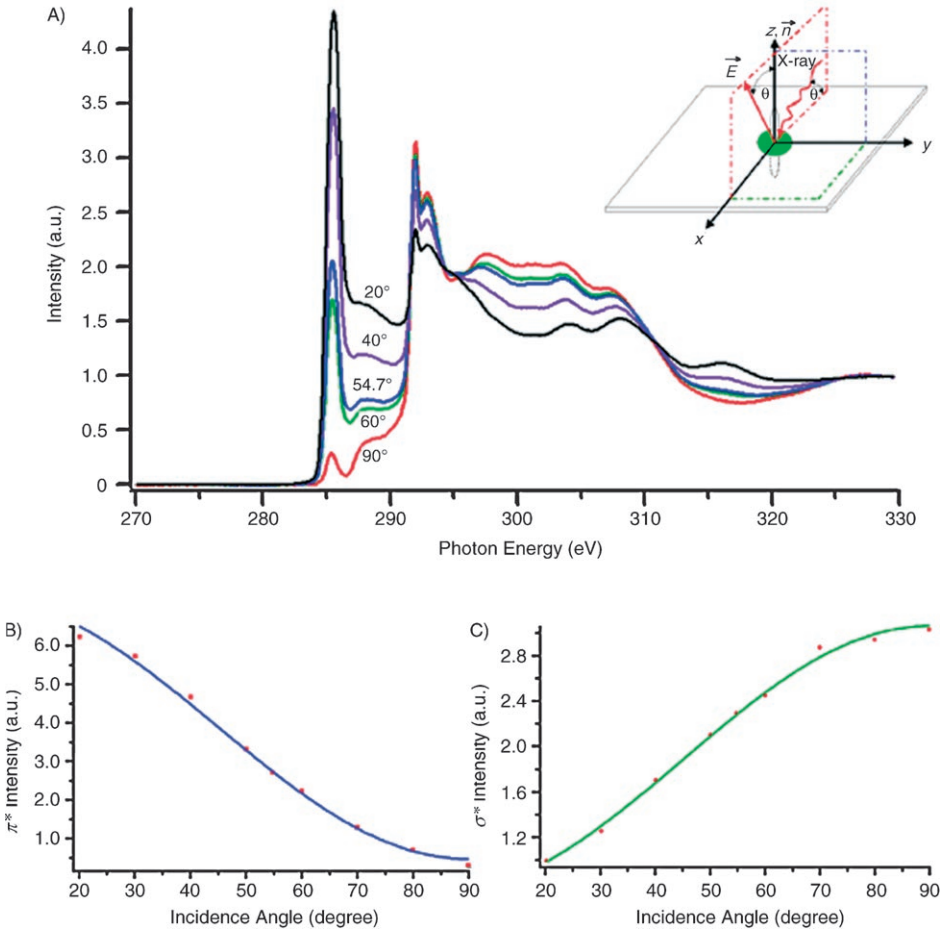

Figure 5. A) C K-edge PEY spectra of freshly cleaved HOPG graphite taken at retarding potentials of −50 V, after rotating the sample in the plane of incidence (intervals from 20° to 90°) to the incident beam. Selected spectra are shown. All the spectra have been pre- and post-edge normalized. The inset shows the geometry of π* vector orbitals and σ* planes with respect to the incident beam and the electric field vector, **E**, which remains perpendicular to the incident X-ray irradiation. B) Integrated intensity of π* resonance at different angles of incidence (the blue line is a fit to the cosine function). C) Integrated intensity of the σ* bound exciton resonance at different angles of incidence (the green line is a fit to a sine-squared function). Intensities of π* and σ* resonances were determined by subtracting an arctan function from the pre- and post-edge normalized spectra to simulate the edge jump, followed by fitting of the π* or σ* peaks with a Gaussian function). Errors in the integrated areas are ±1.5%. Reprinted from Ref. [24].

aligned normal to the *xy*-planar surface, whereas the σ* plane is localized along the surface. As the angle of incidence changes from glancing to normal, the direction of the resultant electric field vector (**E**) changes in the *xz* plane as shown, and always remains perpendicular to the direction of propagation of the incident beam.

The maximum projection of the electric field vector onto a specific orbital, either σ* or π*, will result in maximum peak intensity. Thus, at normal incidence (90°), the electric field vector, which is parallel to the surface and normal to the π* orbitals, will result in a very small projection of the electric field vector onto the π* orbital, implying a corresponding low NEXAFS intensity for the π* resonance and hence, a higher maximum intensity for the σ* resonance (Figure 5). On the other hand, at glancing incidence (20°), the electric field vector has a large projection onto the π* orbitals, resulting in a maximal intensity of the π* resonance and a minimal intensity of the σ* resonance. A plot of the π* intensity versus the incidence angle shows a classic cosine-squared dependence (Figure 5B), whereas a plot of σ* intensity shows a sine-squared dependence with respect to the incidence angle (Figure 5C).[15,24] A similar model has been independently developed by Schiessling et al., based mainly on geometrical considerations, and has been used to study average alignment in MWNT samples.[41]

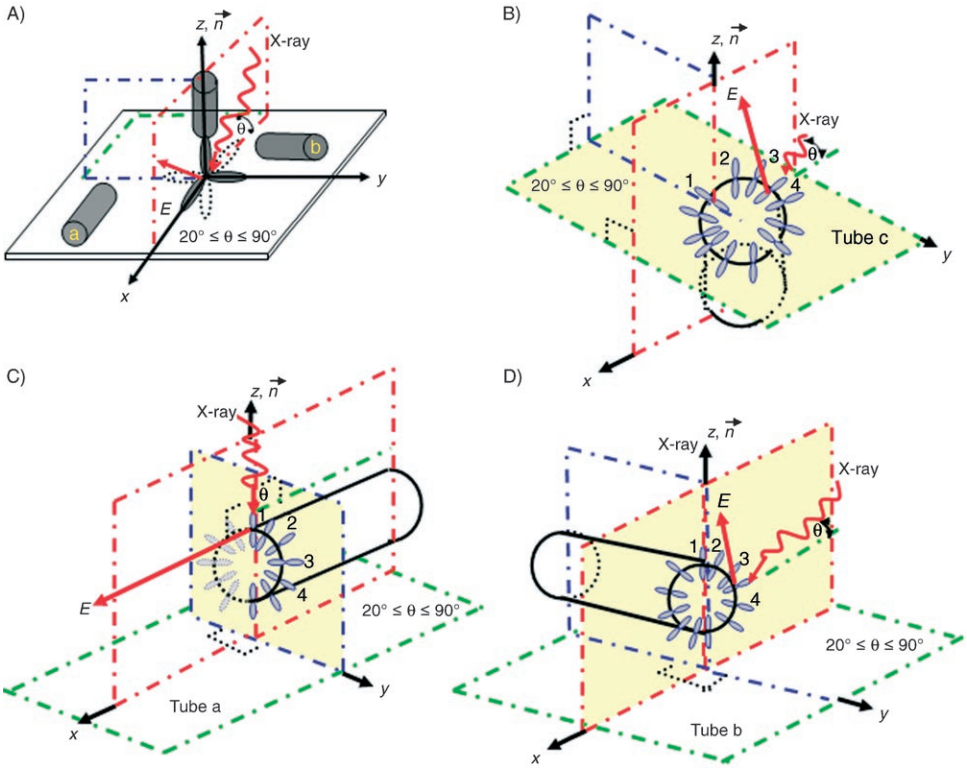

Figure 6. A) Schematic depiction of three possible orientations of nanotubes aligned along Cartesian axes: Tube a (along the *x* axis), Tube b (along the *y* axis), and Tube c (along the *z* axis). The π* orbitals are in the *yz*, *xz*, and *xy* planes, respectively. B–D) Orientations of π* orbitals for each of the different nanotubes with respect to the electric field vector and the incident beam. The angle of incidence changes from glancing (20°) to normal (90°) with the electric field vector always in a perpendicular orientation to the direction of propagation. The incident beam always rotates in the *xz* plane. Please see text for further details. Adapted from Ref. [24].

4.2. Theoretical Modeling of Nanotube NEXAFS Spectra

We have recently developed a model to explain polarization data obtained for HOPG and for carbon nanotube samples, both single- and multi-walled. Herein only the angular dependency trend for π* resonances will be discussed for reasons of simplicity.[24] Figure 6 shows three possible orientations of nanotubes on a surface. In a film comprising a buckypaper of SWNTs, it is expected that nanotubes would be constrained to lie within the *xy* plane of the paper, whereas a random mixture of tubes would be oriented in positions, depicted as Tube a (i.e., a tube lying along *x* axis), Tube b (that is, a tube lying along *y* axis), as well as all conceivable intermediate positions between them in the *xy* plane. In aligned SWNT fibers, all the tubes should point in a specific direction, whereas in arrays or forests of nanotubes, the tubes are expected to point upward and to lie perpendicular to the surface, as shown with Tube c.

Each individual tube (along the individual *x*, *y*, and *z* axes) will demonstrate its own characteristic polarization trend. For instance, it is expected that Tube a will follow the same angular dependency trends as HOPG graphite. That is, at normal incidence, the electric field vector runs along the tube axis and therefore is orthogonal to the π* orbitals, which project out of the tubes and lie in the *yz* plane (Figure 6B). On the other hand, at glancing incidence, the electric field vector has a large projection onto the same plane as the π* orbitals (the *yz* plane). However, despite similar trends with HOPG, it is expected that for the same number of carbon atoms, the HOPG sheet will have a higher π* intensity as compared with that of its nanotube counterpart, due to the electric field vector contributing varying projections onto different π* orbitals in the cylindrical tube. Nonetheless as with HOPG, the π* resonance intensity for Tube a will be the highest at glancing incidence. The predicted anisotropy for an ideal sample consisting only of tubes aligned in the direction of Tube a is shown in Figure 7A (dotted line).[24,40]

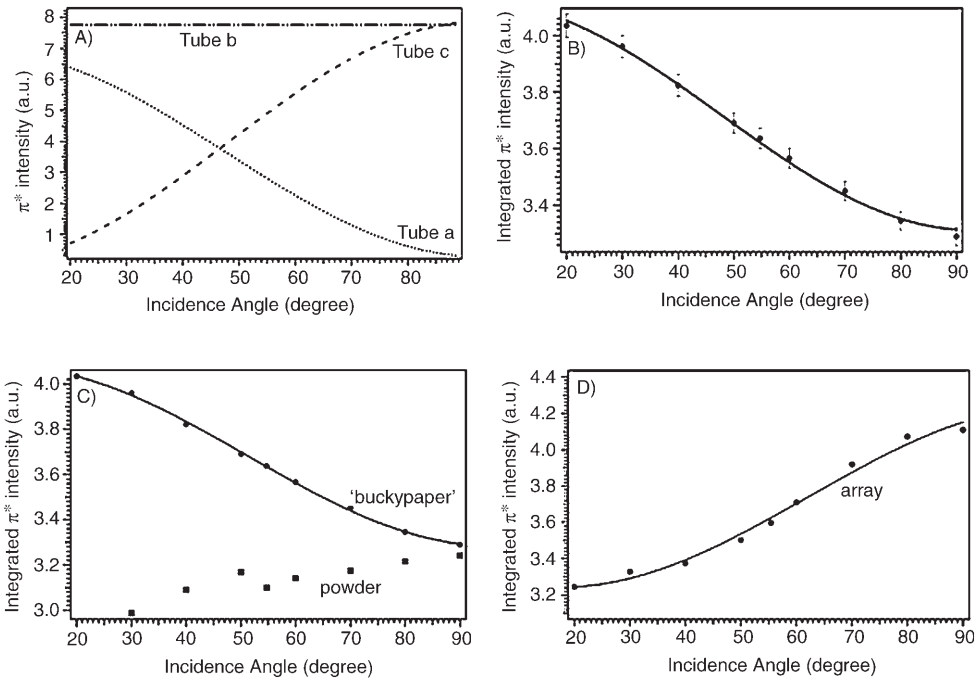

Figure 7. Calculating the proportion of tubes constrained to lie in the plane. A) Dotted line represents the predicted anisotropy for a sample with all the tubes aligned in the direction of Tube a; the dash-dotted line shows the predicted anisotropy for a sample with all the tubes aligned in the direction of Tube b; the dashed line depicts the predicted anisotropy for a sample with all the tubes aligned in the direction of Tube c. B) The filled circles are integrated π* intensities for a SWNT buckypaper at different angles of incidence. The solid line is the weighted sum of the contributions of Tube a (31%), Tube b (56%), and Tube c (13%), which have been fitted to the experimental trend noted for the buckypaper mat. C) Integrated intensity of π* resonances at different angles of incidence. The circles correspond to the SWNT buckypaper, while green squares correspond to SWNT powder. The solid line is a fit to the cosine function. D) Integrated intensities of π* resonances at different angles of incidence. The circles correspond to a 1.5 mm SWNT/MWNT array. The solid line represents a fit to a cosine function (i.e., $I(\theta) = a < M + > b\cos(2(\theta - \gamma))$,?used to determine (b/a) values of normalized amplitude, which are related to the order parameter of the transitional dipole moment. All data are within ±2% error. Reprinted in part from Ref. [24]

4.3. Experimental NEXAFS Observations of Carbon Nanotubes

The above model has recently been confirmed by experimental data. C K-edge spectra were taken for all types of carbon nanotube samples at retarding potentials of −50 V after rotating the sample in the plane of incidence (intervals from 20° to 90°) with respect to the incident beam. All spectra were pre- and post-edge normalized. Thus, changes in spectral intensity observed arise from anisotropy in the system and are independent of total carbon content.[24,40] For comparison, SEM images were taken of each sample studied by NEXAFS spectroscopy; these include nanotube powders, SWNT films or buckypaper, as well as vertically aligned MWNTs and SWNTs.

In any given sample of SWNT and MWNT powder, it is expected that there will be a random combination of tubes oriented along the *x*, *y*, and *z* axes (Tube a, Tube b, and Tube c, respectively) and also in their respective planes (Figure 8A

It is expected that Tube b will show an entirely different angular dependence, as shown in Figure 7A (dash-dotted line). More specifically, at normal or glancing incidence, the electric field vector has exactly the same sum projections onto the π* orbitals, since it is in the same *xz* plane as that of the π* orbitals. Thus, this tube exhibits completely isotropic behavior, which manifests itself as a straight line in a plot of normalized intensity versus angle.

As mentioned above, a SWNT film or buckypaper will consist of nanotubes in randomized positions amongst those of Tube a, Tube b, and intermediate orientations. It should be noted that these films would intrinsically have much lower anisotropy than graphite because of their dissimilarity, both due to intrinsic curvature effects as well as due to disorder within the plane of the buckypaper.

In theory, Tube c is expected to show the reverse trend to that of Tube a and graphite (Figures 6 and 7a). For this tube, which stands upright, at normal incidence, the electric field vector is in the same *xy* plane as the π* orbitals, and thus, the π* resonances will be the highest at this angle, as opposed to at glancing angles. In other words, there is an increase in the intensity of the π* resonance with increasing angle of incidence.

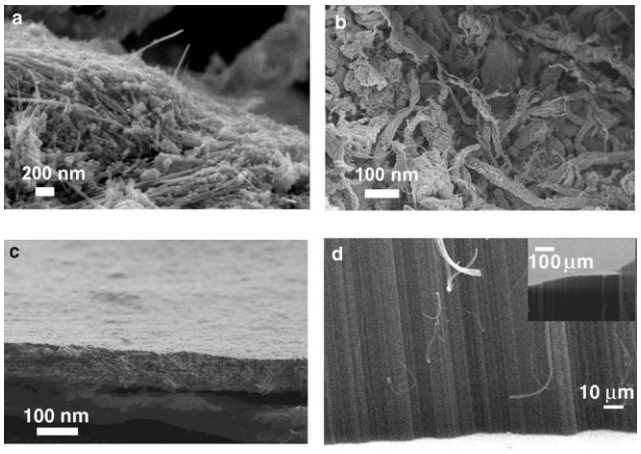

Figure 8. SEM images of A) raw MWNT powder, B) raw SWNT HiPco powder, c) a tilt view of a SWNT buckypaper, and D) an aligned 1.5 mm SWNT/MWNT array with the inset showing the array surface (Reprinted in part from Ref. [24]).

and B). Thus, it is expected that powder samples will possess angular isotropy due to the significant presence of Tube c, which clearly shows the reverse behavior of Tube a and thus will cancel out any angular dependence of tubes oriented in the direction of Tube a.[18,24,40] As a result of the random orientation of tubes in the powder, there will be a lack of any angular polarization trend observed with either the π* or the σ* resonances. This was in fact precisely observed.[24,40]

For the σ* resonances, there does not appear to be a systematic variation in intensity as a function of incidence angle for carbon nanotubes. It is well known that there is significant π* mixing in the σ* and σ*+π* orbitals of HOPG, which is further enhanced in nanotubes due to curvature-induced rehybridization effects. This is apparent in the relative broadening of the so-called bound-exciton peak in nanotubes, as compared with graphite. Thus, for orientation analysis of nanotubes, it is more informative to primarily focus on the π* peak of C K-edge.

For carbon nanotube buckypaper (Figure 8C) and carbon nanotube arrays (Figure 8D), the observed polarization trends, as have been presented above, can be seen as in Figure 7C and D, respectively. For SWNT buckypaper, the remnant HOPG-like anisotropy observed for the π* resonances indicates that there are not a sufficient quantity of upright tubes, exhibiting Tube c-like behavior, to completely cancel out contributions from projections arising from Tube a-like species. Thus, it can be concluded that the tubes have been constrained to lie in the plane of the buckypaper (Tube a and b), thereby introducing detectable anisotropy in the sample. The presence of Tube b-like species accounts for the lower degree of anisotropy as compared with HOPG graphite.

While the behavior observed for a carbon nanotube buckypaper can be attributed to a vectorial combination of Tube a and b-like species, one can assume that for arrays, the presence of primarily Tube c-like species will account for the expected, observed behavior (Figure 7D). An array of SWNTs and MWNTs was studied, as imaged by SEM (Figure 8D). As discussed above, the observed polarization trend of increasing π* resonance intensity with increasing angle of incidence was in fact noted (Figure 7D). A similar analysis has recently been reported for MWNT carpet samples annealed at 1700 to 2000°C.[42] Thus, NEXAFS spectroscopy can be utilized to successfully distinguish amongst a powder nanotube sample, a nanotube buckypaper, and an array of nanotubes. It is also worth noting that the simple models derived in the previous section are remarkably accurate in predicting the behavior of flat tubes (e.g., buckypapers) and upright tubes (e.g., vertical arrays).

In addition, quantitative analysis was performed to determine the actual percentages of Tube a, b, c-like species present in a sample. For example, the experimental plot of the integrated π* intensities for the buckypaper can be fitted to a weighted sum of the functions used for the angular dependencies of Tubes a, b, and c (as shown by the solid line in Figure 7B). This provides a good estimate of the relative contribution of different species to the π* intensities of the buckypaper. Upon deconvolution, we see that only about 13% of the tubes have a Tube c-like orientation. The majority (≈87%) of the tubes are actually constrained to lie in the plane. Tube a-like species and Tube b-like species contribute about 31% and 56%, respectively, to the weighted sum depicted by the solid line. The anisotropy observed in the above experimental data correlate well with the relatively low anisotropy expected for these structures. This further demonstrates the sensitivity of NEXAFS in determining order in these systems.

Furthermore, order parameters can be used to determine the degree of alignment in nanotube buckypaper and arrays. For example, we have used the order parameter (OP), otherwise known as the dichroic ratio,[43,44] defined as:

$$\mathrm{OP} = (I_{\perp} - I_{\parallel})/((I_{\perp} + I_{\parallel})$$

where $I_{\perp}$ is the intensity at normal incidence and $I_{\parallel}$ is the intensity at grazing incidence. Values close to unity indicate higher order. The OP is roughly symmetric about the disorder condition and it is useful for general comparisons. The OP for HOPG was calculated to be −0.902, with the negative sign indicating that the π* resonance decreases in intensity with increasing angle of incidence. From the definition of the order parameters described above, remnant intensity at normal incidence, arising from the presence of Tube B-like species, will result in more disorder and consequently, a smaller order parameter for nanotubes as compared with that seen in graphite. In fact, the OP values for SWNT buckypaper and powder were calculated to be −0.0933 and 0.0407 respectively, indicative of sample anisotropy. Therefore, these order parameters can be used to compare ordering and alignment in films of nanotubes prepared by different methods.[31]

5. Conclusions and Outlook

Successful realization of the use of NEXAFS spectroscopy as a complementary tool in investigating the electronic and structural properties of nanostructures, such as carbon nanotubes, will greatly enhance the fundamental understanding and also, applicability of these nanomaterials. Most importantly, this technique is a nondestructive method of simultaneously probing the structure and surface orientation of nanotubes as well as their surface chemical functionalities, which cannot be easily achieved by many other spectroscopic techniques. We have successfully demonstrated the use of NEXAFS spectroscopy as a multifunctional nanoscale characterization tool that is complementary to conventional microscopy and spectroscopy techniques. In particular, it is an excellent probe of sidewall functionalization.

NEXAFS allows for the following: We can study the surface chemistry and electronic structure of both SWNTs and MWNTs, simultaneously; identify of the phases of non-carbonaceous structures, such as boron nitride (BN) nanotubes; monitor the presence of defects and degree of crystallinity in these nanoscale systems, and ultimately, quantitatively and qualitatively evaluate order and alignment in carbon nanotube-based systems. Moreover, NEXAFS can be used in determining the degree of order in additional nanotube-

based films and fibers, derived from routes including melt processing, electrospinning, metal-assisted deposition, and Langmuir–Blodgett techniques.[45] Future work will focus on in situ observation of the doping and chemical functionalization of carbon nanotubes as well as the determination of order in other aligned nanoscale systems.

Acknowledgements

The authors would like to thank Dr. Zugen Fu for collection of the B_2O_3 calibration NEXAFS spectrum taken at the U7A NIST/DOW beamline, located at the National Synchrotron Light Source (NSLS) at Brookhaven National Laboratory (BNL). We acknowledge support of this work through startup funds provided by the State University of New York at Stony Brook as well as BNL. Acknowledgements are also made to the National Science Foundation (DMII-0403859 and CAREER award DMR-0348239) and to the donors of the Petroleum Research Fund, administered by the American Chemical Society, for support of this research. S.S.W. thanks 3M for a non-tenured faculty award. Research was carried out in part at the NSLS at BNL, which is supported by the US Department of Energy under contract number DE-AC02-98CH10886. Research at Oak Ridge National Laboratory, managed by UT-Batelle, LLC, was sponsored under contract DE-AC05-00OR22725.

[1] P. Avouris, *Acc. Chem. Res.* **2002**, *35*, 1026.
[2] M. S. Dresselhaus, G. Dresselhaus, P. Avouris, *Carbon Nanotubes: Synthesis Structure, Properties, and Applications*; Springer, Berlin, **2001**.
[3] R. H. Baughman, A. A. Zakhidov, W. A. de Heer, *Science* **2002**, *297*, 787.
[4] P. Calvert, *Nature* **1999**, *399*, 210.
[5] P. Dorozhkin, D. Golberg, Y. Bando, Z.-C. Dong, *Appl. Phys. Lett.* **2002**, *81*, 1083.
[6] X. Blase, J. C. Charlier, A. De Vita, R. Car, *Appl. Phys. A* **1999**, *68*, 293.
[7] J. Bahr, J. M. Tour, *J. Mater. Chem.* **2002**, *12*, 1952.
[8] S. Banerjee, M. G. C. Kahn, S. S. Wong, *Chem. Eur. J.* **2003**, *9*, 1898.
[9] A. Hirsch, *Angew. Chem.* **2002**, *114*, 1933; *Angew. Chem. Int. Ed.* **2002**, *41*, 1853.
[10] S. Niyogi, M. A. Hamon, H. Hu, B. Zhao, P. Bhowmik, R. Sen, M. E. Itkis, R. C. Haddon, *Acc. Chem. Res.* **2002**, *35*, 1105.
[11] S. Banerjee, T. Hemraj-Benny, S. S. Wong, *Adv. Mater.* **2005**, *17*, 17.
[12] M. S. Dresselhaus, G. Dresselhaus, A. Jorio, A. G. Souza Filho, M. A. Pimenta, R. Saito, *Acc. Chem. Res.* **2002**, *35*, 1070.
[13] F. L. Coffman, R. Cao, P. A. Pianetta, S. Kapoor, M. Kelly, L. Terminello, *Appl. Phys. Lett.* **1996**, *69*, 568.
[14] M. Holzinger, J. Abraham, P. Whelan, R. Graupner, L. Ley, F. Hennrich, M. Kappes, A. Hirsch, *J. Am. Chem. Soc.* **2003**, *125*, 8556.
[15] J. Stöhr, *NEXAFS Spectroscopy*; Springer, Berlin, **1992**.
[16] C.-C. Chen, A. B. Herhold, C. S. Johnson, A. P. Alivisatos, *Science* **1997**, *276*, 398.
[17] Y. H. Tang, P. Zhang, P. S. Kim, T. K. Sham, Y. F. Hu, X. H. Sun, N. B. Wong, M. K. Fung, Y. F. Zheng, C. S. Lee, S. T. Lee, *Appl. Phys. Lett.* **2001**, *79*, 3773.
[18] Y. H. Tang, T. K. Sham, Y. F. Hu, C. S. Lee, S. T. Lee, *Chem. Phys. Lett.* **2002**, *366*, 636.
[19] A. Kuznetsova, I. Popova, J. T. Yates Jr. , M. J. Bronikowski, C. B. Huffman, J. Liu, R. E. Smalley, H. H. Hwu, J. G. Chen, *J. Am. Chem. Soc.* **2001**, *123*, 10699.
[20] S. Point, T. Minea, B. Bouchet-Fabre, A. Granier, G. Turban, *Diamond Relat. Mater.* **2005**, *14*, 891.
[21] S. Banerjee, T. Hemraj-Benny, M. Balasubramanian, D. A. Fischer, J. A. Misewich, S. S. Wong, *Chem. Commun.* **2004**, 772.
[22] S. Banerjee, T. Hemraj-Benny, M. Balasubramanian, D. A. Fischer, J. A. Misewich, S. S. Wong, *ChemPhysChem* **2004**, *5*, 1416.
[23] T. Hemraj-Benny, S. Banerjee, S. Sambasivan, D. A. Fischer, W. Han, J. A. Misewich, S. S. Wong, *Phys. Chem. Chem. Phys.* **2005**, *7*, 1103.
[24] S. Banerjee, T. Hemraj-Benny, S. Sambasivan, D. A. Fischer, J. A. Misewich, S. S. Wong, *J. Phys. Chem. B* **2005**, *109*, 8489.
[25] S. Banerjee, S. S. Wong, *J. Phys. Chem. B* **2002**, *106*, 12144.
[26] L. C. Teague, S. Banerjee, S. S. Wong, C. A. Richter, J. D. Batteas, **2005**, unpublished results.
[27] K. C. Hwang, *J. Chem. Soc. Chem. Commun.* **1995**, 173.
[28] S. Banerjee, S. S. Wong, *Nano Lett.* **2004**, *4*, 1445.
[29] W. Han, Y. Bando, K. Kurashima, T. Sato, *Appl. Phys. Lett.* **1998**, *73*, 3085.
[30] D. Golberg, Y. Bando, W. Han, K. Kurashima, T. Sato, *Chem. Phys. Lett.* **1999**, *308*, 337.
[31] P. Poulin, B. Vigolo, P. Launois, *Carbon* **2002**, *40*, 1741.
[32] A. B. Dalton, S. Collins, E. Munoz, J. M. Razal, V. H. Ebron, J. P. Ferraris, J. N. Coleman, B. G. Kim, R. H. Baughman, *Nature* **2003**, *423*, 703.
[33] S. Fan, M. G. Chapline, N. R. Franklin, T. W. Tombler, A. M. Cassell, H. Dai, *Science* **1999**, *283*, 512.
[34] S. Huang, L. Dai, A. Mau, *Physica B* **2002**, *323*, 333.
[35] Z. F. Ren, Z. P. Huang, J. W. Xu, J. H. Wang, P. Bush, M. P. Siegal, P. N. Provencio, *Science* **1998**, *282*, 1105.
[36] D. Chattopadhyay, I. Galeska, F. Papadimitrakopoulos, *J. Am. Chem. Soc.* **2001**, *123*, 9451.
[37] M. Ichida, S. Mizuno, H. Kataura, Y. Achiba, A. Nakamura, *Appl. Phys. A* **2004**, *78*, 1117.
[38] P. Launois, A. Marucci, B. Vigolo, P. Bernier, A. Derre, P. Poulin, *J. Nanosci. Nanotechnol.* **2001**, *1*, 125.
[39] O. Lourie, H. D. Wagner, *J. Mater. Res.* **1998**, *13*, 2418.
[40] T. Hemraj-Benny, S. Banerjee, S. Sambasivan, D. A. Fischer, G. Eres, A. A. Puretzky, D. B. Geohegan, D. H. Lowndes, J. A. Misewich, S. S. Wong, **2005**, unpublished results.
[41] J. Schiessling, L. Kjeldgaard, F. Rohmund, L. K. L. Falk, E. E. B. Campbell, J. Nordgen, P. A. Bruehwiler, *J. Phys. Condens. Matter* **2003**, *15*, 6563.
[42] B. Bouchet-Fabre, M. Pinault, V. Pichot, P. Launois, M. Mayne-L'Hermite, P. Parent, K. Laffon, D. Durand, C. Reynaud, *Diamond Relat. Mater.* **2005**, *14*, 881.
[43] W. E. Wallace, D. A. Fischer, K. Efimenko, W. L. Wu, J. Genzer, *Macromolecules* **2001**, *34*, 5081.
[44] W. L. Wu, S. Sambasivan, C. Y. Wang, W. E. Wallace, J. Genzer, D. A. Fischer, *Eur. Phys. J. E* **2003**, *12*, 127.
[45] M. J. Casavant, D. A. Walters, J. J. Schmidt, R. E. Smalley, *J. Appl. Phys.* **2003**, *93*, 2153.

